

Fast-Response Fringe Field Switching LCD with Patterned Common Electrode

Daming Xu*, Haiwei Chen*, Shin-Tson Wu*, Ming-Chun Li**, Seok-Lyul Lee**, and Wen-Ching Tsai**

*College of Optics and Photonics, University of Central Florida, Orlando, FL 32816, USA

** AU Optronics Corp., Hsinchu Science Park, Hsinchu 300, Taiwan

Abstract

A fast-response and wide-view fringe-field switching LCD using patterned common electrodes is proposed. By applying a restoring pulse voltage on common electrodes, LC decay process is expedited. The GTG decay time can be reduced by $>7X$, depending on the applied erasing voltage. This new mode also preserves the wide-view characteristics as the conventional FFS mode. It is attractive for reducing motion blurs.

Author Keywords

Fringe field switching, liquid crystal display, fast response.

1. Introduction

Fringe field switching (FFS) LCD [1-3] has been widely used in high-end display products because of its high transmittance, wide view, and pressure-resistance for touch panels. However, some technical barriers, such as TFT charging time for high resolution LCDs [3], image sticking [4] and slow response time, remain to be overcome.

The response time of a FFS LCD is mainly determined by the LC material and cell gap. Compared to turn-on process, which is driven by electric field, the decay process is usually slower since it is mainly governed by the elastic restoring force. Because the twist elastic constant K_{22} of LC is relatively small, the decay time of FFS LCD with $3\text{-}\mu\text{m}$ cell gap is usually $\sim 20\text{ms}$ [5]. In order to reduce response time, various approaches have been proposed [5-7]. However, each approach has its own pros and cons. Hence, there is urgent need to develop a fast-switching FFS LCD without sacrificing its attractive features.

In this paper, we propose a patterned common electrode FFS mode, denoted as PC-FFS, to achieve fast response time. The bright state and the dark state are achieved by applying fringe fields along different directions. With a restoring voltage pulse to expedite the decay process, we are able to achieve $>7X$ faster gray-to-gray (GTG) decay time than conventional FFS LCD.

2. Device Structure

Figs. 1(a) and 1(b) depict the top view of a conventional FFS and proposed PCFFS cell, respectively. In the FFS cell, pixel electrodes are stripe-shaped while common electrode is planar. Both are formed on the bottom substrate with a passivation layer in between. However, in the PCFFS cell, the bottom common electrodes are also fabricated to be stripe shape, setting at an angle α w.r.t. the x axis. Same as FFS cells, for the purpose of achieving low driving voltage the homogeneous rubbing angle is set at 10° and 80° w.r.t. the x axis for PCFFS cells using a negative (n-PCFFS) and positive (p-PCFFS) LC, respectively [2]. The cell gap is optimized at $\lambda = 550\text{ nm}$ with $d\Delta n = 360\text{ nm}$ for n-PCFFS and 380 nm for p-PCFFS to obtain high transmittance.

To achieve bright state, a driving voltage is applied to the pixel electrodes while common electrodes are grounded. Same as the

FFS mode, fringe fields with strong horizontal components are generated here to reorient the LC directors. Hence, the incident light accumulates phase retardation and transmits through the analyzer. During decay process, the pixel electrodes are floated while a restoring voltage pulse is applied between adjacent common electrodes. The electric potential of floated pixel electrodes are spontaneously determined by the restoring voltage [8]. The in-plane field generated by this restoring voltage would exert a strong torque to pull the LC directors back to their initial rubbing [6, 9]. Hence, the decay process is accelerated and faster decay time is obtained.

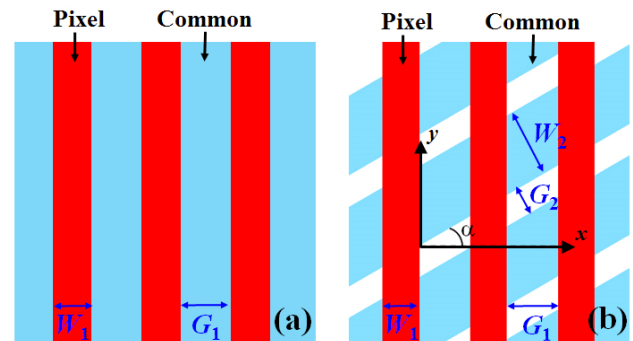


Figure 1. Device structure of (a) conventional FFS and (b) PCFFS modes.

3. Simulation Results: VT Characteristics

The device performance are studied and optimized by using commercial simulator TechWiz LCD (Sanayi, Korea) and the electro-optic properties are calculated by the extended 2×2 Jones matrix method. To make a fair comparison between FFS and PCFFS cells, we use the same device configurations: pixel electrode width $W_1 = 2\mu\text{m}$, electrode gap $G_1 = 3\mu\text{m}$, pretilt angle 2° . The passivation layer between the pixel and common electrodes is Si_3N_4 ($\epsilon = 7.5$, thickness = 150nm) whereas the alignment layer is 80-nm thick polyimide ($\epsilon = 3.8$). The physical properties of the positive and negative LC materials studied are listed in Table I. The negative LC material UCF-N2 was developed by our group [10], while the positive $\Delta\epsilon$ LC DIC-LC3 is a commercial material from DIC Japan [11].

TABLE I. Physical properties of two LC mixtures studied ($T = 23^\circ\text{C}$ and $\lambda = 550\text{ nm}$).

LC	γ_1 (mPa·s)	$\Delta\epsilon$	Δn	K_{11} (pN)	K_{22} (pN)	K_{33} (pN)
UCF-N2	94.7	-3.8	0.117	15.8	7.2	14.0
DIC-LC3	62.0	9.0	0.111	10.9	5.6	13.8

(a) VT Curves: Fig. 2 shows the simulated voltage-dependent transmittance (VT) curves of FFS and PCFFS cells employing a positive or a negative $\Delta\epsilon$ LC material. Here, the α angle is set at 10° and -20° for PCFFS cells employing p- and n-PCFFS, respectively. The values of α angle are optimized to achieve the

fastest response time, as will be explained later. The dimension of common electrodes is: $W_2 = 4\mu\text{m}$ and $G_2 = 2\mu\text{m}$. It is shown that both p- and n-PCFFS cells have nearly identical VT curves to the corresponding FFS cells. This is a very attractive feature as the proposed PCFFS can achieve similar high transmittance as FFS does at the same voltage.

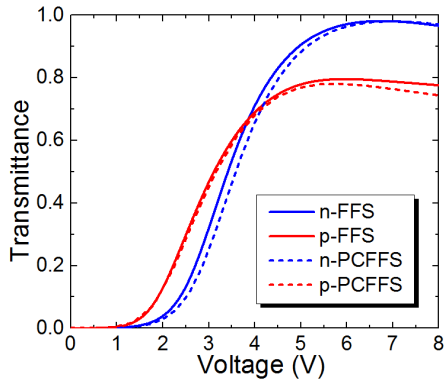


Figure 2. Simulated VT curves of the FFS and PCFFS modes using positive and negative LCs ($\lambda = 550\text{nm}$).

(b) Viewing Angle: In order to widen the viewing angle of both modes, compensation films are required. In simulations, both modes were compensated by a half-wave biaxial film [12], whose parameters are $n_x = 1.521$, $n_y = 1.519$, $n_z = 1.520$ and thickness is $137.5\ \mu\text{m}$. The n_x axis is perpendicular to the rubbing direction. Figs. 3(a) and 3(b) plot the viewing angle of film-compensated p-FFS and p-PCFFS modes, respectively. Due to space limitation, only the results of LC modes employing positive LC are shown here; however, those using negative LC exhibit the same trend. We can see that both p-FFS and p-PCFFS possess an over 85° viewing zone with contrast ratio greater than 100:1, while p-PCFFS shows slightly better viewing angle than p-FFS. Since their dark state is identical due to the same alignment, cell gap, and polarizers, the contrast ratio mainly depends on the bright state. The fields generated by the patterned common electrodes in the p-PCFFS cell create multi-domain LC distribution at the bright state [13], thus rendering the viewing angle wider.

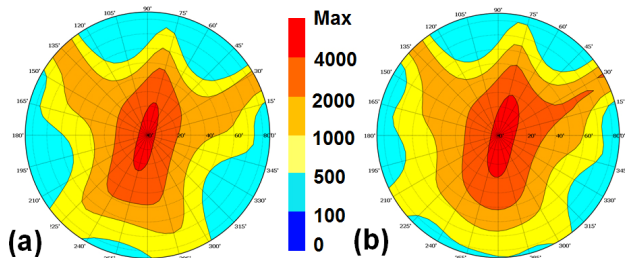


Figure 3. Isocontrast plots of biaxial film-compensated (a) p-FFS and (b) p-PCFFS cells ($\lambda = 550\ \text{nm}$).

(c) Fabrication Tolerance: Our PCFFS modes possess a larger fabrication tolerance. Firstly, the VT characteristics of the PCFFS mode are insensitive to the α angle. Figs. 4(a)-(d) compare the on-state transmittance profiles of p-PCFFS cells using different α angles with that of a conventional p-FFS cell, and the numerical values of peak transmittance (T_{max}) and on-state voltage (V_{on}) are listed in Table II. It clearly shows that when α angle increases from -30° , 10° to 45° , both T_{max} and V_{on} remain nearly unchanged. The same trend applies to n-PCFFS as

well. This insensitivity to α angle implies that we have a large tolerance in device fabrication because a small error in α angle would not influence the VT characteristics of PCFFS cells. Secondly, the VT curves of PCFFS cells are also insensitive to the dimension of bottom common electrodes within a certain range. Fig. 5 shows the dependences of T_{max} and V_{on} on the G_2/W_2 ratio of p-PCFFS. They are both insensitive to the G_2/W_2 ratio when $G_2/W_2 \leq 1.0$. This feature indicates a small difference in G_2/W_2 would not affect the VT characteristics of p-PCFFS cells as long as it is kept below 1.0. Beyond this region, T_{max} decreases and V_{on} increases dramatically. The same trend applies to n-PCFFS as well, but the tolerance range is even larger: $G_2/W_2 \leq 1.5$, showing that n-PCFFS is less sensitive to the G_2/W_2 ratio than p-PCFFS. This is due to the positive LC directors tend to follow the electric field direction, which is determined by G_2/W_2 ratio.

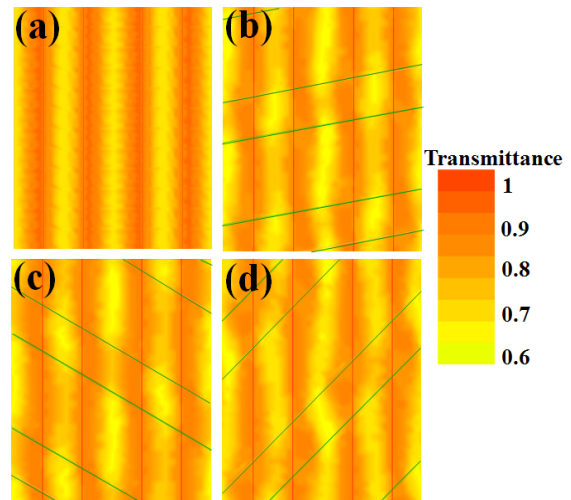


Figure 4. On-state transmittance profiles of (a) p-FFS, and p-PCFFS modes with different α angles: (b) $\alpha = 10^\circ$, (c) $\alpha = -30^\circ$ and (d) $\alpha = 45^\circ$ ($\lambda = 550\ \text{nm}$).

TABLE II. Simulated V_{on} and T_{max} of p-FFS and p-PCFFS modes with different α angles ($\lambda = 550\text{nm}$).

LC Cell	V_{on} (V)	T_{max}
p-FFS	5.6	81.9%
p-PCFFS $\alpha = 10^\circ$	5.5	81.4%
p-PCFFS $\alpha = -30^\circ$	5.5	81.7%
p-PCFFS $\alpha = 45^\circ$	5.5	81.2%

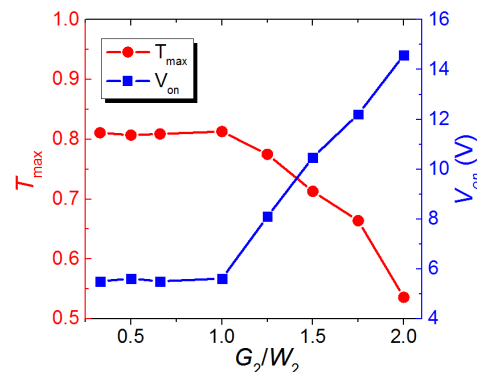


Figure 5. The dependences of T_{max} and V_{on} on the G_2/W_2 ratio for p-PCFFS mode.

In brief, the proposed PCFFS mode exhibits nearly identical VT characteristics with the conventional FFS mode and it possesses a large fabrication tolerance. More attractively, it can achieve a much faster response time than FFS mode, as outlined below.

4. Simulation Results: Dynamic Response

(a) Response Time: During the decay process, a restoring voltage pulse is applied between adjacent common electrodes while the top pixel electrodes are kept floated. Hence, the in-plane field generated by the restoring voltage would pull the LC directors back to their initial states. Note that the value of α angle is very crucial to the decay time. Take p-PCFFS as an example, the optimal α angle for achieving the fastest decay time is 10° . In the full-bright state, the LC directors are reoriented at $\sim 40^\circ$ - 50° from their initial alignment direction φ [2]. Thus, the value of α angle should be optimized within the range $\varphi - 90^\circ < \alpha < \varphi - 45^\circ$ in order to maximize the restoring torque experienced by the LCs. In simulations, we set the rubbing angle of p-PCFFS at $\varphi = 80^\circ$. Accordingly, α angle should be optimized between -10° and 35° .

Fig. 6(a) depicts the time-transmittance (TT) curves of the p-PCFFS cells with α increasing from -10° , 10° to 30° . Despite the rise time is not emphasized in this study, our PCFFS cell still shows faster turn-on time than p-FFS cell (14.15 vs. 20.62ms). During the relaxation process, a 15V restoring voltage is applied to the common electrodes in the p-PCFFS cells. Although α angle does not influence the VT curves, it determines the decay processes. By setting α at 10° , we are able to achieve the fastest decay time, which is $\sim 2.6X$ faster than that of conventional FFS mode (6.14 vs. 16.22 ms). Moreover, if a material with reduced viscosity is employed [5], the cell gap can be further reduced and response time will become even shorter for PCFFS modes.

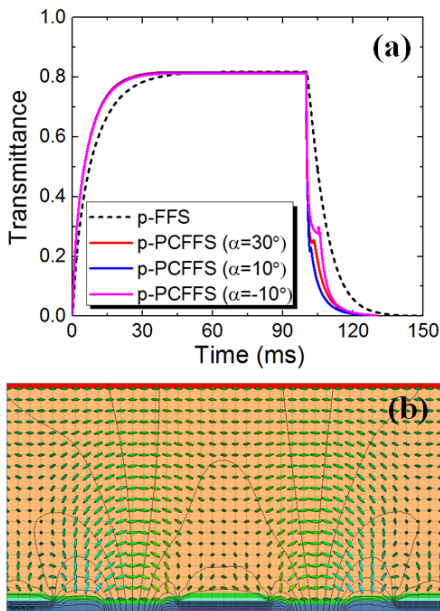


Figure 6. (a) The response time of p-FFS and p-PCFFS mode with different α angles; and (b) electric potential profiles of p-PCFFS when a restoring voltage is applied.

Note the decay processes of PCFFS show double relaxation processes: the fast relaxation caused by the short restoring pulse is followed by a slow decay process from the spontaneous relaxation of LCs. This is because only the horizontal electric

field is effective in pulling the LC back to its original alignment direction. The effective restoring torque on the top of common electrodes is almost zero because the electric fields in these regions are mainly along the vertical direction, as shown in Fig. 6(b). Thus, by only applying the restoring voltage, the first faster decay process cannot reach dark state. If the transmittance of final level during a decay process is lower than the lowest transmittance the first decay process could reach, the second spontaneous relaxation process is required.

Similarly, by applying a restoring pulse, the decay time of n-PCFFS can be dramatically reduced as well. Different from p-PCFFS, α is set at -20° in n-PCFFS to achieve the fastest decay time, which is $>2X$ faster than conventional n-FFS mode (7.4ms vs.16.9ms). Thus, by applying the restoring pulse for a short period, the decay time of both p- and n-PCFFS can be shortened.

(b) Passivation Layer Effect: The restoring electric field is generated between top pixel and bottom common electrodes by penetrating through the passivation layer during decay process. Due to the dielectric properties of passivation layer [14], part of the applied voltage is shielded. Thus, a higher restoring voltage is required to accelerate the decay process. Fig. 7(a) illustrates the field intensity profiles in two PCFFS cells with $0.40\text{-}\mu\text{m}$ and $0.15\text{-}\mu\text{m}$ passivation layers when a 15V restoring voltage is applied. It clearly shows that the field penetrates deeper into the LC bulk in the cell with $0.15\text{-}\mu\text{m}$ passivation whereas the voltage is more shielded in the other cell by the $0.40\text{-}\mu\text{m}$ passivation layer. To better understand their difference, we investigated the field intensity change at point A, where the field is mainly along horizontal direction, as shown in Fig. 7(b). Because more voltage is shielded by the passivation layer, the penetration depth of the in-plane field is much shallower in the $0.40\text{-}\mu\text{m}$ passivation cell than that in the other one. Therefore, a thinner passivation is preferred to reduce the restoring voltage. If we can reduce the passivation thickness to $0.10\mu\text{m}$, the required restoring voltage would be further reduced to 10V.

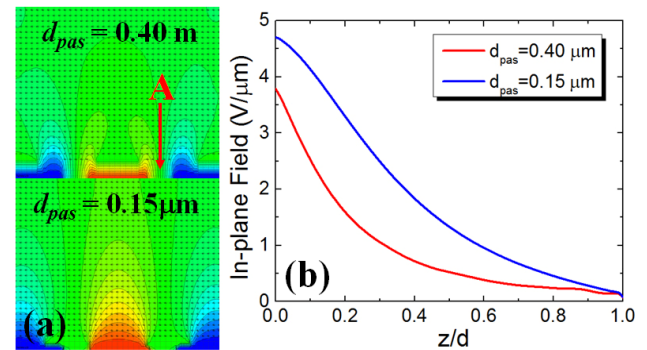


Figure 7. (a) Field intensity profiles in PCFFS cells with different passivation thickness; and (b) the distribution of in-plane field in the cell at point A.

(c) GTG Decay Time: To evaluate the GTG decay time, we divided the VT curve uniformly into 8 gray levels (G0-G7). As usual, the decay time is defined as 90%-10% transmittance change. The restoring pulse is applied to bottom common electrodes for a short period until the transmittance decays to the designated gray level. Then a bias voltage is applied to hold the transmittance at the targeted final gray level. Details of this driving method have been reported in some prior works [15, 16].

The TT curves of the p-PCFFS decay processes from G7 to lower gray levels are shown in Fig. 8. The decay time of the first

relaxation process expedited by the electric field is very fast, while the decay processes to lower gray levels (G0 and G1) require a longer time for the elastic relaxation of LC directors to accomplish. The calculated GTG decay time of p-PCFFS is summarized in Table III. Most GTG decay times are below 1ms except those whose final level is G0 or G1, and the average GTG decay time is 2.82ms at 23°C. Compared to the p-FFS cell, whose average GTG response time is 22.75ms [13], our PCFFS cell shows >8X faster GTG decay time. Furthermore, the decay time can be reduced if LC with a lower viscosity [5] is used.

The GTG decay time of n-PCFFS mode was also calculated, as listed in Table IV. Compared with the conventional n-FFS mode, the proposed n-PCFFS mode is able to achieve >7X faster GTG decay time (3.21 vs. 24.05ms) at 23°C. This GTG decay time is even faster than that of MVA LCDs [17], whose GTG response time is ~5ms. Hence, this mode exhibits promising applications in eliminating motion blurs for fast-response LCDs.

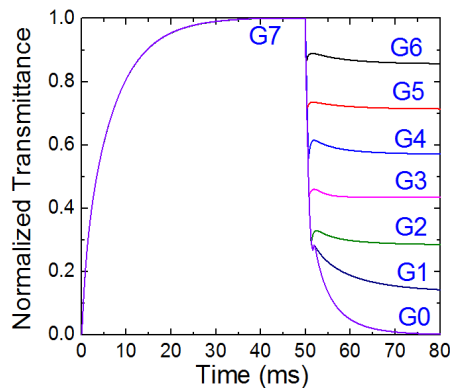


Figure 8. TT curves of the decay processes from G7 to lower gray levels and their response times.

TABLE III. Calculated GTG decay time of p-PCFFS at T = 23°C and $\lambda = 550$ nm (Unit: ms).

Level	0	1	2	3	4	5	6
0							
1	5.48						
2	5.62	4.88					
3	6.04	4.98	0.47				
4	6.04	5.02	0.51	0.33			
5	6.10	5.04	0.62	0.47	0.29		
6	6.08	5.04	0.73	0.59	0.43	0.24	
7	6.14	5.08	0.88	0.77	0.54	0.39	0.31

TABLE IV. Calculated GTG decay time of n-PCFFS at T = 23°C and $\lambda = 550$ nm (Unit: ms).

Level	0	1	2	3	4	5	6
0							
1	5.76						
2	6.17	4.87					
3	6.58	5.33	0.32				
4	6.81	5.61	0.53	0.37			
5	7.09	5.83	0.92	0.64	0.29		
6	7.15	5.97	1.11	0.75	0.53	0.31	
7	7.43	6.23	1.39	0.84	0.63	0.37	0.25

5. Conclusion

We proposed a new PCFFS mode to achieve fast decay time. Compared to conventional FFS mode, the PCFFS mode exhibits nearly identical VT performance and possess a large fabrication

tolerance. By applying a restoring voltage pulse on the adjacent common electrodes, the average GTG decay time is reduced by >8X for p-PCFFS and >7X for n-PCFFS; as compared to FFS. This fast-response mode has potential applications for reducing motion picture image blurs.

6. References

- [1] S. H. Lee, S. L. Lee, H. Y. Kim, "Electro-optic characteristics and switching principle of a nematic liquid crystal cell controlled by fringe-field switching," *Applied Physics Letters* **73**, 2881-2883 (1998).
- [2] Y. Chen, Z. Y. Luo, F. L. Peng, S. T. Wu, "Fringe-Field Switching with a Negative Dielectric Anisotropy Liquid Crystal," *J. Disp. Technol.* **9**, 74-77 (2013).
- [3] D. H. Kim, Y. J. Lim, D. E. Kim, H. Ren, S. H. Ahn, S. H. Lee, "Past, present, and future of fringe-field switching-liquid crystal display," *Liq. Cryst.* **15**, 99-106 (2014).
- [4] D. Xu, F. Peng, H. Chen, J. Yuan, S. T. Wu, M. C. Li, S. L. Lee, W. C. Tsai, "Image sticking in liquid crystal displays with lateral electric fields," *J. Appl. Phys.* **116**, 193102 (2014).
- [5] H. Chen, F. Peng, Z. Luo, D. Xu, S. T. Wu, M. C. Li, S. L. Lee, W. C. Tsai, "High performance liquid crystal displays with a low dielectric constant material," *Opt. Mater. Express* **4**, 2262-2273 (2014).
- [6] D. Xu, L. Rao, C. D. Tu, S. T. Wu, "Nematic liquid crystal display with submillisecond grayscale response time," *J. Disp. Technol.* **9**, 67-70 (2013).
- [7] C. Y. Xiang, X. W. Sun, X. J. Yin, "The electro-optic properties of a vertically aligned fast response liquid crystal display with three-electrode driving," *J. Phys. D: Appl. Phys.* **37**, 994-997 (2004).
- [8] M. K. Park, S. W. Oh, J. S. Park, D. J. Lee, K. H. Park, J. H. Lee, B. K. Kim, H. R. Kim, "Mixed-field-switching liquid crystal mode using in-plane and fringe fields self-adjusted by bottom floating electrode for transmittance enhancement," *Liq. Cryst.* **41**, 908-919 (2014).
- [9] D. J. Channin, "Triode optical gate: A new liquid crystal electro-optic device," *Appl. Phys. Lett.* **11**, 603-605 (1975).
- [10] Y. Chen, F. Peng, T. Yamaguchi, X. Song, S. T. Wu, "High performance negative dielectric anisotropy liquid crystals for display applications," *Crystals* **3**, 483-503 (2013).
- [11] H. Takatsu, "Advanced liquid crystal materials for active matrix displays," *Conf. Proc. Advanced Display Materials and Devices*, 43 (2014).
- [12] Z. Luo, D. Xu, S. T. Wu, "Emerging quantum-dots-enhanced LCDs," *J. Disp. Technol.* **10**, 526-539 (2014).
- [13] D. Xu, H. Chen, S. T. Wu, M. C. Li, S. L. Lee, W. C. Tsai, "A fringe field switching liquid crystal display with fast grayscale response time," *J. Disp. Technol.* **11**, 353-359 (2015).
- [14] M. Jiao, Z. Ge, Q. Song, S. T. Wu, "Alignment layer effects on thin liquid crystal cells," *Appl. Phys. Lett.* **92**, 061102 (2008).
- [15] Y. Li, Z. Ge, R. Lu, M. Jiao, S. T. Wu, "Fast-response liquid-crystal displays using crossed fringe fields," *J. Soc. Inf. Disp.* **16**, 1069-1074 (2008).
- [16] J. W. Kim, T. H. Choi, T. H. Yoon, "Drive schemes for sub-millisecond switching of LCD panels," *SID Int. Symp. Dig. Tech. Pap.* **45**, 1460-1462 (2014).
- [17] A. Takeda, S. Kataoka, T. Sasaki, H. Chida, H. Tsuda, K. Ohmuro, T. Sasabayashi, Y. Koike, K. Okamoto, "A super-high image quality multi-domain vertical alignment LCD by new rubbing-less technology," *SID Int. Symp. Dig. Tech. Pap.* **29**, 1077-1100 (1998).